Bounds on metamaterials: theoretical results

Kristensson, Gerhard; Sohl, Christian; Larsson, Christer; Gustafsson, Mats

2008

Bounds on Metamaterials — Theoretical Results

G. Kristensson, C. Sohl, C. Larsson, and M. Gustafsson

Department of Electrical and Information Technology, Lund University
P.O. Box, SE-221 00 Lund, Sweden

Abstract— A dispersion relation for the combined effect of scattering and absorption of electromagnetic waves is presented for a large class of linear and passive material models. By invoking the optical theorem, the result states that the extinction cross section integrated over all frequencies is related to the static polarizability dyadics. In particular, it is established that the integrated extinction is the same for all materials having identical static properties, irrespectively whether the permittivity or the permeability have negative real parts at non-zero frequencies or not. This condition implies bounds on scattering and absorption by metamaterials, and several numerical illustrations that verify these results are presented in the paper.

1. BACKGROUND

In a series of papers [13–16], the holomorphic properties of the forward scattering amplitude have been exploited and experimentally verified. As a result, a sum rule for the extinction cross section is established. This outcome hinges on the physical principles of causality and energy conservations — both well established and tested — and relates the (weighted) integrated extinction to the static material properties of the obstacle. A rather intriguing consequence of this sum rule is that the static properties measure the broadband scattering and absorption strengths of the obstacle. This fact implies a renaissance for polarizability analyzes of obstacles, but also an appreciation of the large efforts made in the past, and that now prove helpful, see *e.g.*, [7, 17].

The extinction sum rule naturally introduces bounds on the scattering and the absorption features of an obstacle — a component that is further developed and numerically illustrated in this paper. This attribute has also been used in antenna applications to give new bounds on the product of gain and bandwidth of antennas of arbitrary shape [4, 12]. The sum rule has been verified numerically for single scatterers — with materials that show dispersion or not [13, 14]. It has also been verified experimentally in several ways [15]. In this paper we employ a non-connected geometry, which show multiple scattering and allow for two different materials to interact. As a result, new interesting bounds on scattering and absorption are developed.

The paper also illustrates — in a non-trivial way — D. S. Jones' rather unknown results [5, 6]. These results by D. S. Jones, which simply state that the eigenvalues of the polarizability properties of a scatterer increase monotonically with increasing material parameters, deserve a wider attention. In a series of numerical computations, using the null field approach [11], we verify these results.

2. A SUM RULE FOR EXTINCTION

This section sets the notation of the problem and states the main theoretical results used in this paper, but no proofs are given. For proofs we refer to the pertinent published papers [13, 14].

Consider the direct scattering problem of a plane electromagnetic wave $\boldsymbol{E}\exp\{\mathrm{i}k\hat{\boldsymbol{k}}\cdot\boldsymbol{x}\}$ (time dependence $\exp\{-\mathrm{i}\omega t\}$) impinging in the $\hat{\boldsymbol{k}}$-direction on a target embedded in free space. The wave number in free space is denoted by $k=\omega/\mathrm{c}_0$. The target can be a single scatterer or it may consist of several non-connected parts. The material of the scatterer is modeled by a set of linear and passive constitutive relations which are assumed to be invariant under time translations (*i.e.*, stationary constitutive relations). The scattering dyadic $\mathbf{S}$ is independent of $\boldsymbol{E}$, and it is defined in terms of the scattered electric field $\boldsymbol{E}_{\mathrm{s}}$ as [2, 9, 18]

$$\mathbf{S}(k;\hat{\boldsymbol{k}}\curvearrowright\hat{\boldsymbol{x}})\cdot\boldsymbol{E}=\lim_{x\to\infty}x\mathrm{e}^{-\mathrm{i}kx}\boldsymbol{E}_{\mathrm{s}}(k;\boldsymbol{x})$$

where $x=|\boldsymbol{x}|$ denotes the magnitude of the position vector, and $\hat{\boldsymbol{x}}=\boldsymbol{x}/x$. A target's overall scattering properties are commonly quantified by the scattering cross section σ_{s}, defined as the total power scattered in all directions divided by the incident power flux. The extinction cross

section $\sigma_{\rm ext} = \sigma_{\rm s} + \sigma_{\rm a}$ is defined as the sum of the scattering and absorption cross sections, where the latter is a measure of the absorbed power in the target [2, 18]. The extinction cross section is also determined from the knowledge of the scattering dyadic in the forward direction, $\hat{\boldsymbol{x}} = \hat{\boldsymbol{k}}$, *viz.*,

$$\sigma_{\rm ext}(k;\hat{\boldsymbol{k}},\hat{\boldsymbol{e}}) = \frac{4\pi}{k}\,{\rm Im}\left\{\hat{\boldsymbol{e}}^*\cdot\mathbf{S}(k;\hat{\boldsymbol{k}}\curvearrowright\hat{\boldsymbol{k}})\cdot\hat{\boldsymbol{e}}\right\} \tag{1}$$

where an asterisk denotes the complex conjugate, and the electric polarization $\hat{\boldsymbol{e}} = \boldsymbol{E}/|\boldsymbol{E}|$. Relation (1) is known as the optical theorem or forward scattering theorem, and it is applicable to many different wave phenomena such as acoustic waves, electromagnetic waves, and elementary particles [16].

A dispersion relation for the combined effect of scattering and absorption of electromagnetic waves is derived in Ref. 13 from the holomorphic properties of the forward scattering dyadic. One of the underlying assumptions of the result is that the forward scattering is causal, *i.e.*, the scattered field must not proceed the incident field in the forward direction. The result is a sum rule of the extinction cross section valid for a large class of linear and passive targets:[1]

$$\int_0^\infty \frac{\sigma_{\rm ext}(k;\hat{\boldsymbol{k}},\hat{\boldsymbol{e}})}{k^2}\,{\rm d}k = \frac{\pi}{2}\left(\hat{\boldsymbol{e}}^*\cdot\boldsymbol{\gamma}_{\rm e}\cdot\hat{\boldsymbol{e}} + (\hat{\boldsymbol{k}}\times\hat{\boldsymbol{e}}^*)\cdot\boldsymbol{\gamma}_{\rm m}\cdot(\hat{\boldsymbol{k}}\times\hat{\boldsymbol{e}})\right) \tag{2}$$

where $\boldsymbol{\gamma}_{\rm e}$ and $\boldsymbol{\gamma}_{\rm m}$ denote the electric and magnetic polarizability dyadics, respectively [7, 17]. This identity holds for all scatterers satisfying the assumption above, and it constitutes the main theoretical result used in this paper. This rather intriguing result has far-reaching consequences on how much an obstacle scatters and absorbs, and it also quantifies the interaction between parts with different materials.

The sum rule (2) can also be estimated from below by integrating over a finite frequency interval $K \in [0,\infty)$, *i.e.*,

$$\int_K \frac{\sigma(k;\hat{\boldsymbol{k}},\hat{\boldsymbol{e}})}{k^2}\,{\rm d}k \le \frac{\pi}{2}\left(\hat{\boldsymbol{e}}^*\cdot\boldsymbol{\gamma}_{\rm e}\cdot\hat{\boldsymbol{e}} + (\hat{\boldsymbol{k}}\times\hat{\boldsymbol{e}}^*)\cdot\boldsymbol{\gamma}_{\rm m}\cdot(\hat{\boldsymbol{k}}\times\hat{\boldsymbol{e}})\right)$$

where σ denotes any of the cross sections $\sigma_{\rm ext}, \sigma_{\rm s}$, and $\sigma_{\rm a}$.

The extinction cross section $\sigma_{\rm ext}$ measures the total interaction of the incident plane wave with the obstacle, and the integral on the left-hand side of (2) provides a measure of the overall scattering and the absorption properties of the obstacle. As a consequence of (2), large scattering or absorption effects, *i.e.*, a large left-hand side of (2), call for large electric and/or magnetic polarizability dyadics. In other applications, like cloaking, the extinction effects must be small (at least in a finite frequency interval) and the electric and magnetic polarizability dyadics have to be as small as possible for a given volume. In both cases, the static properties act as a measure of the dynamic effects. We also immediately conclude that all scatterers having the same right-hand side, *i.e.*, polarizability properties, have the same integrated extinction.

The effects of (2) are exploited in this paper, and in a few numerical examples we illustrate that two materials with the same static properties have identical integrated extinction. Several of these examples show metamaterial characteristics, *i.e.*, the material has temporally dispersive material parameters where both the real parts of the permittivity and the permeability are negative in the same frequency interval. In all cases it is the static properties of the obstacle that determine the integrated scattering properties of the obstacle.

3. MATERIAL MODELING

Material modeling plays an important role in making realistic computer simulations. This is especially important in modeling the broadband electric and magnetic behavior of the scatterer. In particular, the models have to be consistent with the causality assumptions made above. As a consequence, the material models have to satisfy the Kramers-Kronig relations [3, 8].

All materials show dispersive effects over a sufficiently large frequency interval. In this paper we make frequent use of the Lorentz model, which models the resonance behavior of many solid materials. The relative permittivity of the Lorentz model is:

$$\epsilon(\omega) = \epsilon_\infty - \frac{\omega_{\rm p}^2}{\omega^2-\omega_0^2+{\rm i}\omega\nu} = \epsilon_\infty - \frac{(\omega_{\rm p}a/{\rm c}_0)^2}{(ka)^2-(\omega_0 a/{\rm c}_0)^2+{\rm i}ka(\nu a/{\rm c}_0)} \tag{3}$$

[1] A similar, but less developed, sum rule has been reported in the literature, see *e.g.*, [10, p. 423].

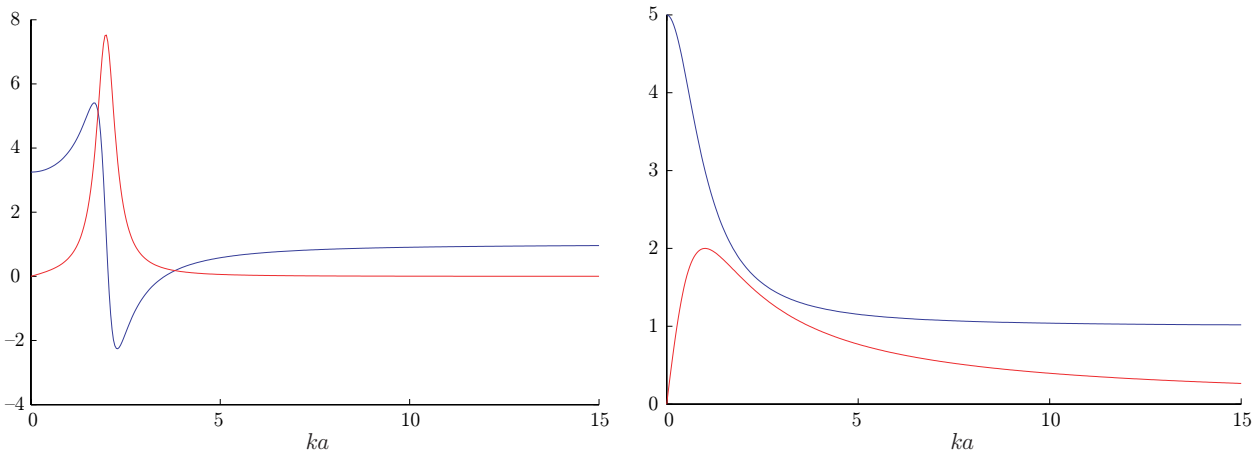

Figure 1: The real (blue curve) and imaginary (red curve) parts of the Lorentz and the Debye models, respectively, as a function of the dimensionless frequency parameter ka. See Table 1 for the explicit numerical values of the parameters.

The positive constant ϵ_∞ is the optical response of the permittivity, and the constant ω_p is the plasma frequency that models the strength of the dispersion. The resonance frequency of the model is determined by the angular frequency, ω_0, and the collision frequency $\nu > 0$. With appropriate choice of the material parameters, the real part of the permittivity becomes negative. The explicit value of the permittivity in the static limit ($\omega = 0$) is

$$\epsilon(0) = \epsilon_\infty + \frac{\omega_\mathrm{p}^2}{\omega_0^2}$$

A similar model is also used for the relative permeability μ. The Lorentz model employed in this paper has the parameters given in Table 1, and it is illustrated on the left-hand side in Figure 1.

Lorentz	
ϵ_∞	1
$\omega_\mathrm{p} a/\mathrm{c}_0$	3
$\omega_0 a/\mathrm{c}_0$	2
$\nu a/\mathrm{c}_0$	0.6

Drude	
ϵ_∞	1
$\omega_\mathrm{p} a/\mathrm{c}_0$	3
$\omega_0 a/\mathrm{c}_0$	0
$\nu a/\mathrm{c}_0$	0.6

Debye	
ϵ_∞	1
ϵ_s	5
$\tau \mathrm{c}_0/a$	1

Table 1: The material parameters used in the numerical illustrations.

The Drude model is a special case of the Lorentz model for which $\omega_0 = 0$, *i.e.*,

$$\epsilon(\omega) = \epsilon_\infty - \frac{\omega_\mathrm{p}^2}{\omega(\omega + \mathrm{i}\nu)} = \frac{\epsilon_\infty(\omega^2 + \nu^2) - \omega_\mathrm{p}^2}{\omega^2 + \nu^2} + \mathrm{i}\frac{\omega_\mathrm{p}^2 \nu}{\omega(\omega^2 + \nu^2)}$$

This choice implies that the real part of the permittivity is negative over a large frequency interval, *i.e.*, $\omega^2 \leq \omega_\mathrm{p}^2/\epsilon_\infty - \nu^2$. This model is used to describe the dispersive behavior of metamaterials, and at low frequencies it shows strong affinity with the conductivity model, *i.e.*,

$$\epsilon(\omega) = \epsilon_\infty + \mathrm{i}\frac{\varsigma}{\epsilon_0 \omega}$$

In fact, the conductivity $\varsigma = \epsilon_0 \omega_\mathrm{p}^2/\nu$ can be identified from Drude's model.

We also adopt the Debye model, *i.e.*,

$$\epsilon(\omega) = \epsilon_\infty + \frac{\epsilon_\mathrm{s} - \epsilon_\infty}{1 - \mathrm{i}\omega\tau} = \epsilon_\infty + \frac{\epsilon_\mathrm{s} - \epsilon_\infty}{1 - \mathrm{i}ka(\tau \mathrm{c}_0/a)} \tag{4}$$

which is suitable for *e.g.*, polar liquids. The positive constants ϵ_∞ and ϵ_s are the high frequency (optical response) and the static values of the permittivity, respectively. The relaxation time is denoted by $\tau > 0$. The Debye model used in this paper has the parameters given in Table 1, and it is illustrated on the right-hand side of Figure 1.

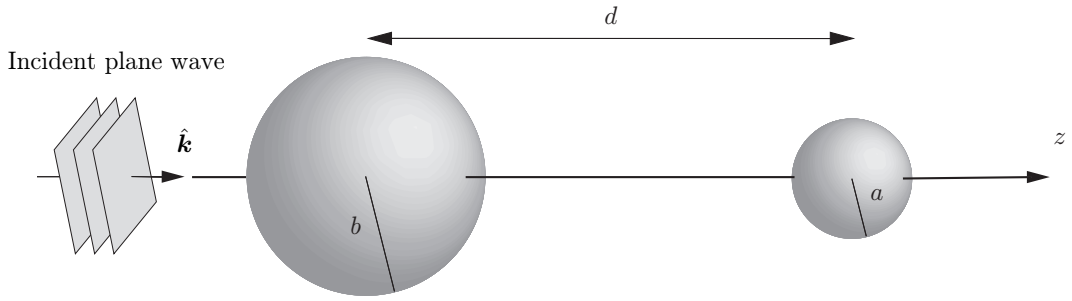

Figure 2: The geometry of the two spheres. The sphere with radius a is located at $d\hat{\boldsymbol{z}}/2$ and the sphere with radius b is located at $-d\hat{\boldsymbol{z}}/2$. The direction of the incident wave in all examples is $\hat{\boldsymbol{k}} = \hat{\boldsymbol{z}}$.

4. NUMERICAL ILLUSTRATIONS — TWO SPHERES

In this section, we illustrate the theoretical results presented in Section 2 in a series of numerical examples using the material models described in Section 3. The scattering geometry consists of two spheres, radii a and b, respectively, and it is illustrated in Figure 2. This geometry, which is a simple example of a non-connected scatterer, is motivated by its potential to have an independent variation of the material parameters in its constitutive parts. In all examples, the plane wave impinges along the symmetry axis of the scatterer with an electric polarization $\hat{\boldsymbol{e}}$ in the x-y-plane, which can be either a real- or a complex-valued unit vector. All frequencies are measured in the dimensionless parameter $\kappa = ka$, and all cross sections are scaled with $2\pi a^2$. The identity in (2), then reads

$$\int_0^\infty \frac{\sigma_{\text{ext}}(\kappa; \hat{\boldsymbol{k}}, \hat{\boldsymbol{e}})}{\kappa^2}\, \mathrm{d}\kappa = \frac{\pi}{3} \frac{1}{4\pi a^3/3} \left(\hat{\boldsymbol{e}}^* \cdot \boldsymbol{\gamma}_{\text{e}} \cdot \hat{\boldsymbol{e}} + (\hat{\boldsymbol{k}} \times \hat{\boldsymbol{e}}^*) \cdot \boldsymbol{\gamma}_{\text{m}} \cdot (\hat{\boldsymbol{k}} \times \hat{\boldsymbol{e}}) \right) \tag{5}$$

The numerical computations in this paper utilize the null-field approach, which is an efficient method to evaluate scattering by non-connected objects [11].

4.1. Computations of the polarizability dyadics

We have seen that the polarizability dyadics are of paramount importance in quantifying the interaction of the plane wave with the scatterer. The electric and magnetic polarizability dyadics are obtained in the same way, so it suffices to employ a computational technique for the electric case — the computations of the magnetic polarizability dyadic then follows analogously.

The electric polarizability dyadic is accessible as an analytic expression for a limited set of canonical bodies, *e.g.*, a homogenous, isotropic dielectric sphere of radius a with static permittivity $\epsilon(0)$ has the polarizability dyadic $\boldsymbol{\gamma}_{\text{e}}$ [17]

$$\boldsymbol{\gamma}_{\text{e}} = 3 \frac{\epsilon(0) - 1}{\epsilon(0) + 2} \frac{4\pi a^3}{3} \mathbf{I}$$

where $\mathbf{I}$ denotes the unit dyadic. Fortunately, for other more complex geometries, the polarizability dyadic is easy to compute using *e.g.*, an finite element (FEM) solver. In the dielectric case, (relative) permittivity $\epsilon(\boldsymbol{x})$, a static boundary value problem has to be solved for the finite scattering volume V, which might consist of several parts. For a given constant complex-valued direction $\hat{\boldsymbol{e}}$, we solve the following explicit problem for the dimensionless generic field $\boldsymbol{F}$:

$$\begin{cases} \nabla \cdot (\epsilon(\boldsymbol{x}) \boldsymbol{F}(\boldsymbol{x})) = 0, \quad \boldsymbol{x} \in V \\ \nabla \cdot \boldsymbol{F}(\boldsymbol{x}) = 0, \quad \boldsymbol{x} \notin V \\ \boldsymbol{F} \to \hat{\boldsymbol{e}} \text{ as } x \to \infty \end{cases}$$

and the projected part of the electric polarizability dyadic $\boldsymbol{\gamma}_{\text{e}}$ is then found by evaluating

$$\boldsymbol{\gamma}_{\text{e}} \cdot \hat{\boldsymbol{e}} = \iiint_V (\epsilon(\boldsymbol{x}) \boldsymbol{F}(\boldsymbol{x}) - \hat{\boldsymbol{e}})\, \mathrm{d}v$$

The high-contrast polarizability dyadic $\boldsymbol{\gamma}_\infty$ is obtained by solving an exterior Dirichlet boundary value problem for the (normalized) surface charge density ρ_{S}, under the condition that the total

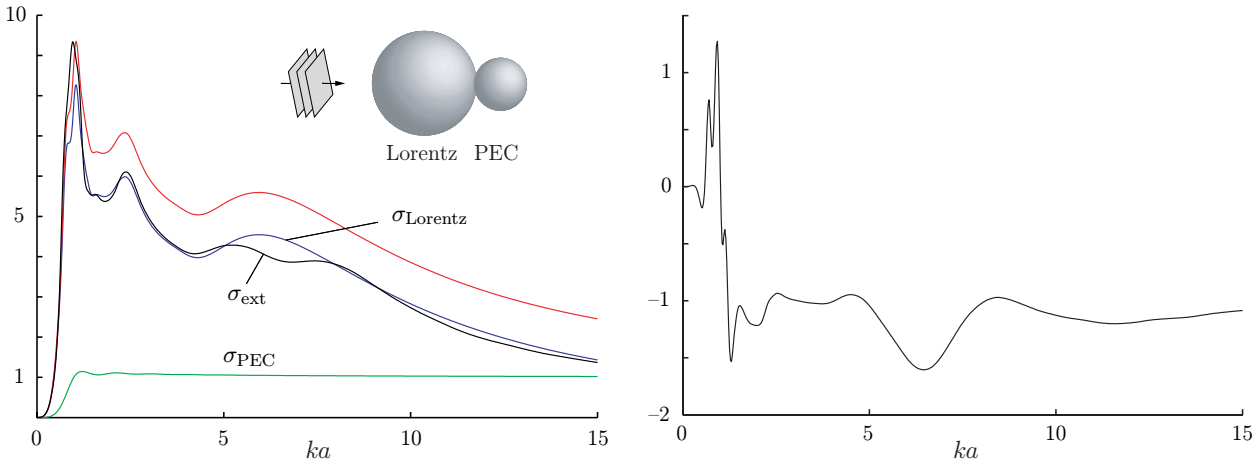

Figure 3: **Left figure:** The black curve shows the extinction cross section σ_{ext} of a PEC sphere (radius a) and a touching ($d = 3a$) non-magnetic Lorentz sphere (radius $b = 2a$) as a function of ka. The red curve shows the extinction cross section of the two spheres without interaction, *i.e.*, the sum of the two individual cross sections, which are shown in green (PEC sphere, σ_{PEC}) and blue (Lorentz sphere, σ_{Lorentz}) curves. **Right figure:** The difference in extinction cross sections between σ_{ext} and $\sigma_{\text{PEC}} + \sigma_{\text{Lorentz}}$. All cross sections are normalized with $2\pi a^2$.

charge on each isolated body is zero. The projected part of the electric polarizability dyadic $\boldsymbol{\gamma}_\infty$ is then obtained by computing

$$\boldsymbol{\gamma}_\infty \cdot \hat{\boldsymbol{e}} = \iint_S \boldsymbol{x}\,(\hat{\boldsymbol{\nu}}(\boldsymbol{x}) \cdot \epsilon(\boldsymbol{x})\boldsymbol{F}(\boldsymbol{x}))\ \mathrm{d}S$$

where S is the bounding surface of V and $\hat{\boldsymbol{\nu}}$ its outward pointing unit normal vector. We refer to *e.g.*, [17] for details on these computations.

For an axially symmetric obstacle, the eigenvalues of the polarizability dyadic are degenerated. Two eigenvalues — corresponding to a static excitation perpendicular to the symmetry axis — are identical and denoted γ below, and one eigenvalue is in general different — corresponding to a static excitation along the symmetry axis.

4.2. PEC and Lorentz spheres

The extinction cross section σ_{ext} for a perfectly electric conduction (PEC) sphere, radius a, and a Lorentz sphere, radius $b = 2a$, is illustrated in Figure 3. The distance between the spheres is $d = 3a$, *i.e.*, the spheres are touching each other. The Lorentz sphere contains a non-magnetic material, $\mu = 1$. The extinction cross section of this geometry is compared with the extinction cross sections obtained for two non-interacting spheres (the sum of the extinction cross sections of the two isolated spheres, red curve), as well as the extinction cross sections of each of the two spheres alone, σ_{Lorentz} and σ_{PEC} (blue and green curves, respectively). All cross sections are normalized with $2\pi a^2$.

The contributions of the electric and the magnetic polarizability dyadics in this example are, see also Section 4.1,

$$\hat{\boldsymbol{e}}^* \cdot \boldsymbol{\gamma}_{\text{e}} \cdot \hat{\boldsymbol{e}} = 12.65\frac{4\pi a^3}{3}, \qquad (\hat{\boldsymbol{k}} \times \hat{\boldsymbol{e}}^*) \cdot \boldsymbol{\gamma}_{\text{m}} \cdot (\hat{\boldsymbol{k}} \times \hat{\boldsymbol{e}}) = -\frac{3}{2}\frac{4\pi a^3}{3}$$

The magnetic part originates from the PEC sphere, which contributes with a factor $-3/2$ times the volume of the sphere. With the normalization used in this paper, the right-hand side of (5) then becomes $\pi(12.65 - 1.5)/3 = 11.68$. This figure is retrieved with almost 3 digits (11.61) using numerical integration on the left-hand side of (5) over the frequency interval in Figure 3. The polarizability dyadic contributions from the PEC and Lorentz spheres alone are

$$\hat{\boldsymbol{e}}^* \cdot \boldsymbol{\gamma}_{\text{e}} \cdot \hat{\boldsymbol{e}} = 3\frac{\epsilon(0) - 1}{\epsilon(0) + 2}\frac{4\pi b^3}{3} = \frac{72}{7}\frac{4\pi a^3}{3}\ \text{(Lorentz)}, \qquad \begin{cases} \hat{\boldsymbol{e}}^* \cdot \boldsymbol{\gamma}_{\text{e}} \cdot \hat{\boldsymbol{e}} = 3\dfrac{4\pi a^3}{3} \\ (\hat{\boldsymbol{k}} \times \hat{\boldsymbol{e}}^*) \cdot \boldsymbol{\gamma}_{\text{m}} \cdot (\hat{\boldsymbol{k}} \times \hat{\boldsymbol{e}}) = -\dfrac{3}{2}\dfrac{4\pi a^3}{3} \end{cases} \text{(PEC)}$$

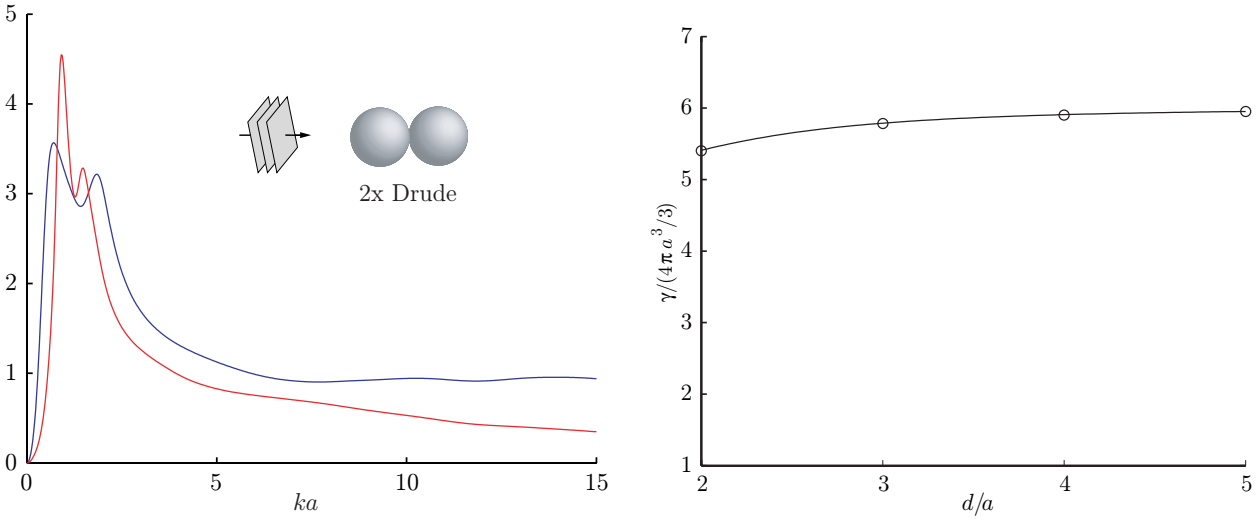

Figure 4: **Left figure:** The extinction cross section of two equal, touching ($d = 2a$) Drude spheres (radii $a = b$) as a function of ka. The blue curve shows the extinction cross section for $\epsilon = \mu$, and the red curve shows the extinction cross section in the case when both spheres are non-magnetic, $\mu = 1$. Both cross sections are normalized with $2\pi a^2$. **Right figure:** The polarizability, γ normalized with $4\pi a^3/3$, for the same geometry as a function of the separation distance d. The circles illustrate the numerical values, and the analytic expression at $d/a = 2$ is $9\zeta(3)/2$.

The integrated extinction of the right curve in Figure 3 then becomes $11.68 - 24\pi/7 - \pi/2 = -0.66$. The corresponding numerically integrated value is -0.63.

We anticipate that the normalized extinction cross section curves σ_{ext}, $\sigma_{\text{Lorentz}} + \sigma_{\text{PEC}}$, and σ_{PEC} at high frequencies all converge to 1, which is twice the projected geometrical cross section area of the PEC sphere. This is in agreement with the extinction paradox [18], and it also shows that the Lorentz sphere becomes invisible at high frequencies as predicted. The curves also clearly illustrate the shadowing effects of the large Lorentz sphere in front of the PEC sphere, *i.e.*, the single PEC sphere assumes its asymptotic value at a much lower frequency than if the obstructing Lorentz sphere is present.

The difference $\sigma_{\text{ext}} - \sigma_{\text{Lorentz}} - \sigma_{\text{PEC}}$ is depicted to the right in Figure 3. This curve shows that the interaction for some frequencies is larger than the sum of the two separate spheres, but at most frequencies the interaction is smaller. This is in agreement with the fact that in the static limit, the electric dipole moment of the Lorentz sphere has a depolarizing effect on the PEC sphere.

4.3. Two identical Drude spheres

In this example, the extinction cross section of two identical, touching Drude spheres (radii $a = b$ and $d = 2a$), is computed for two material settings. In the first setting $\epsilon = \mu$ at all frequencies, *i.e.*, a material that shows metamaterial characteristics at low frequencies, and in the second setting both spheres are non-magnetic, $\mu = 1$. The result is showed to the left in Figure 4. Explicit values of the permittivities are given in Table 1.

The contribution to both the electric and the magnetic polarizability dyadics in the case $\epsilon = \mu$ is [19]

$$\hat{\boldsymbol{e}}^* \cdot \boldsymbol{\gamma}_{\text{e}} \cdot \hat{\boldsymbol{e}} = (\hat{\boldsymbol{k}} \times \hat{\boldsymbol{e}}^*) \cdot \boldsymbol{\gamma}_{\text{m}} \cdot (\hat{\boldsymbol{k}} \times \hat{\boldsymbol{e}}) = \frac{9}{2}\zeta(3)\frac{4\pi a^3}{3}$$

where $\zeta(z)$ is the Riemann zeta-function [1]. The non-magnetic spheres have no magnetic contribution, but only an electric contribution. The right-hand side of (5) for the two curves in Figure 4 therefore assumes the values $3\pi\zeta(3) = 11.33$ and $3\pi\zeta(3)/2 = 5.66$, respectively. These figures are retrieved using numerical integration over the frequency interval in Figure 4 with 3 digits (11.3 and 5.66, respectively). It is intriguing to conclude that these numbers are independent of all the material parameters of the Drude spheres, *i.e.*, independent of ϵ_∞, ω_{p}, and ν.

A further verification of the integrated extinction in (5) is presented to the right in Figure 4. This figure shows the analytically computed polarizability, γ, of two identical Drude spheres [19] as a function of the separating distance d. The values obtained by numerical integration are shown with circles.

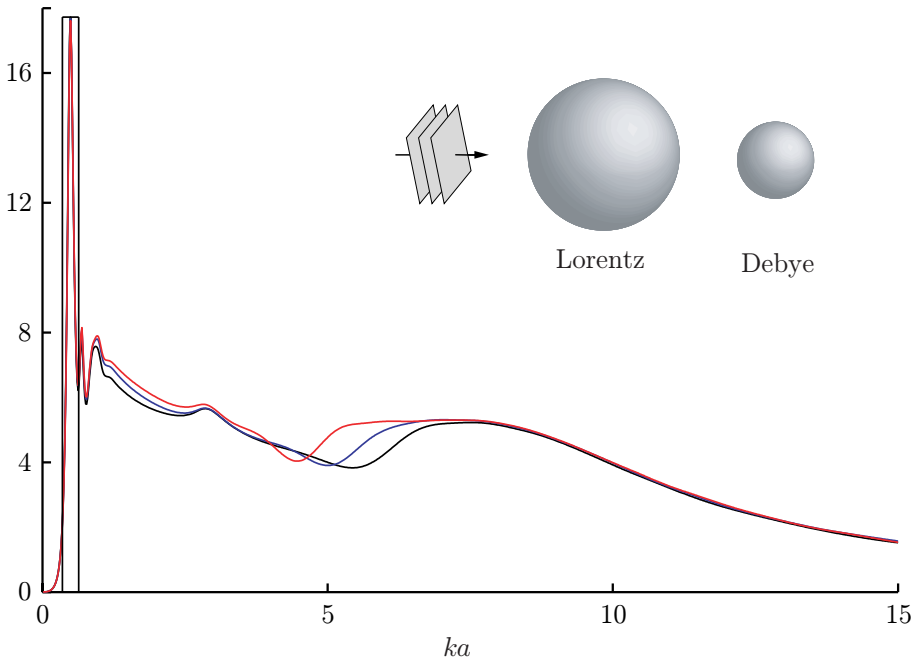

Figure 5: The extinction cross section of a Debye sphere (radius a) and a Lorentz sphere (radius $b = 2a$) with varying separation distances $d = 3a$ (black curve), $d = 4a$ (blue curve), $d = 5a$ (red curve) as a function of ka. The Debye sphere is non-magnetic $\mu = 1$, while the Lorentz sphere has $\mu = \epsilon$. All cross sections are normalized with $2\pi a^2$.

4.4. Debye and Lorentz spheres

The extinction cross section of a Debye sphere (radius a) and a Lorentz sphere (radius $b = 2a$) with varying separation distance $d = 3a, 4a, 5a$ is depicted in Figure 5. The two spheres have material parameters given in Table 1. The Debye sphere is non-magnetic, $\mu = 1$, and the Lorentz sphere has the same permittivity and permeability, *i.e.*, $\epsilon = \mu$.

The contributions of the electric and the magnetic polarizability dyadics are

$$\begin{cases} \hat{\boldsymbol{e}}^* \cdot \boldsymbol{\gamma}_{\mathrm{e}} \cdot \hat{\boldsymbol{e}} = 11.63 \dfrac{4\pi a^3}{3}, & d = 3a \\ \hat{\boldsymbol{e}}^* \cdot \boldsymbol{\gamma}_{\mathrm{e}} \cdot \hat{\boldsymbol{e}} = 11.83 \dfrac{4\pi a^3}{3}, & d = 4a \\ \hat{\boldsymbol{e}}^* \cdot \boldsymbol{\gamma}_{\mathrm{e}} \cdot \hat{\boldsymbol{e}} = 11.91 \dfrac{4\pi a^3}{3}, & d = 5a \end{cases}, \qquad (\hat{\boldsymbol{k}} \times \hat{\boldsymbol{e}}^*) \cdot \boldsymbol{\gamma}_{\mathrm{m}} \cdot (\hat{\boldsymbol{k}} \times \hat{\boldsymbol{e}}) = \frac{72}{7} \frac{4\pi a^3}{3}, \quad d = 3a, 4a, 5a$$

The magnetic part has a contribution from the Lorentz sphere only. With the normalization used in this paper, the right-hand side of (5) then becomes 22.95, 23.16, and 23.24 for the different separation distances. These figure are retrieved using numerical integration over the frequency interval in Figure 5 with almost 3 digits (22.8, 23.0, and 23.2, respectively).

In Figure 5, a box of the same weighted area as the black curve is inserted. This box displays a restriction of the extinction cross section — no scatterer, with the same right-hand side of (5) as the black curve, can lie above the box at all frequencies. To this end, the weighted areas under the curves, which are determined by the static properties, restrict the scattering and absorption strengths of the scatterer — large scattering or absorption can only occur in a small frequency interval.

4.5. Two different materials with the same integrated extinction

We end the numerical illustrations by a computation of the extinction cross sections for two different sets of material parameters with identical static values. Two touching, $d = 3a$, non-magnetic Lorentz spheres, radii a and $b = 2a$, respectively, are used. The result is displayed in Figure 6. The blue curve shows the extinction cross section when the two spheres have materials as given in Table 1. The red curve shows the extinction cross section for two Lorentz spheres both having

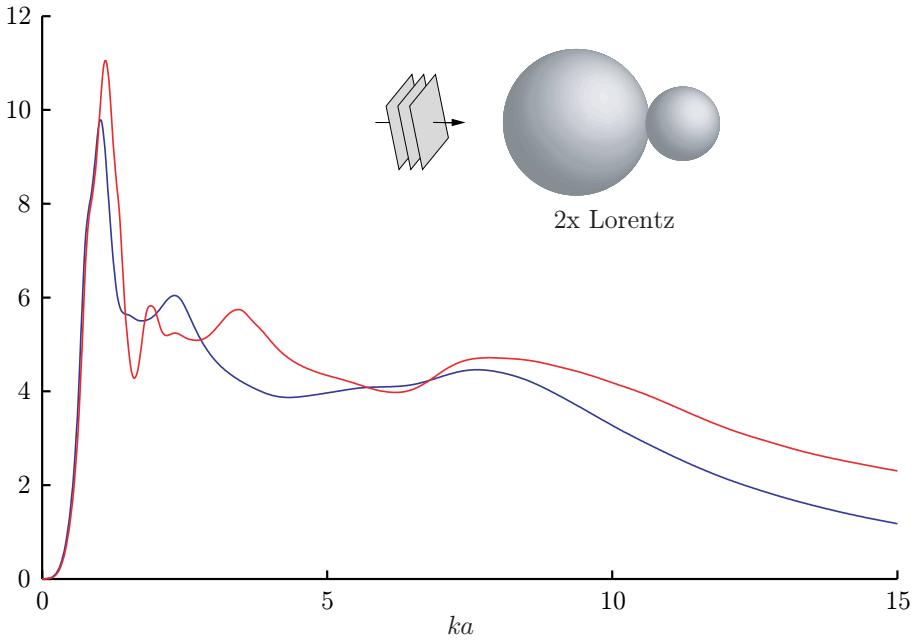

Figure 6: The extinction cross section of two touching Lorentz spheres as a function of ka. Both spheres have identical material parameters and they are non-magnetic, $\mu = 1$, with radii a and $b = 2a$. The data of the blue curve is given in Table 1, and the data of the red curve is $\omega a/\mathrm{c}_0 = 4.5$ and $\omega_0 a/\mathrm{c}_0 = 3$. All cross sections are normalized with $2\pi a^2$.

parameters $\omega a/\mathrm{c}_0 = 4.5$ and $\omega_0 a/\mathrm{c}_0 = 3$. These two sets of materials have a static permittivity of $\epsilon(0) = 13/4$, and therefore the same right-hand side of (5).

The polarizability dyadic contributions from the two Lorentz spheres are the same, *i.e.*,

$$\hat{\boldsymbol{e}}^* \cdot \boldsymbol{\gamma}_{\mathrm{e}} \cdot \hat{\boldsymbol{e}} = 11.29 \frac{4\pi a^3}{3}$$

The right-hand side of (5) then becomes 11.82 in both cases. The integrated extinction is computed using numerical integration over the frequency interval in Figure 6. The results are 11.8 and 11.7, respectively, for the two curves.

5. ILLUSTRATIONS OF D. S. JONES' RESULTS

Sphere 1	$\epsilon(0)$	**Sphere 2**	$\hat{\boldsymbol{e}}^* \cdot \boldsymbol{\gamma}_{\mathrm{e}} \cdot \hat{\boldsymbol{e}}/(4\pi a^3/3)$
Lorentz	13/4	Lorentz	11.29
Debye	5	Lorentz	11.63
PEC	∞	Lorentz	12.65

Table 2: The eigenvalues of the electric polarizability of the Lorentz examples in Section 4. The second Lorentz sphere has the same static permittivity $\epsilon(0) = 13/4$ in all three examples.

The numerical examples shown in Section 4 can be used to illustrate the effect of altering the static properties of the obstacle in a different way. In Table 2, we collect the electric polarizability values of the Lorentz examples in Section 4. These values clearly illustrate D. S. Jones' result [6], which states that the polarizability eigenvalues increase with increasing static permittivity of the scatterer. An immediate consequence of D. S. Jones' result is that a scatterer with larger static material parameters implies a larger right-hand side of (5), and, consequently, a stronger scatterer, as measured by the left-hand side of (5).

The example in Section 4.2 also illustrates that the eigenvalues of the polarizability increase if more material is added to the scatterer. The polarizability of the PEC and Lorentz spheres is 11.15 (in the units used above), whereas the PEC and Lorentz spheres alone have polarizability 1.5 and 72/7, respectively, which both are smaller values.

6. CONCLUSIONS

The sum rule of the extinction cross section (2) have been exploited, and some of its consequences have been discussed. This sum rule holds for a large class of linear and passive material models, and assumes causality and energy conservation via the optical theorem. The result states that the extinction cross section integrated over all frequencies is related to the static polarizability dyadics. In particular, the integrated extinction is the same for all materials having identical static properties, irrespectively of their dynamic properties, as long as they are passive and satisfy causality. Several numerical illustrations verify this sum rule, and, in particular, we illustrate the bounds on the scattering and the absorption properties of the obstacle. Moreover, D. S. Jones' less known results on the dependence of polarizability on the material parameters have been verified.

ACKNOWLEDGMENT

The research reported in this paper is sponsored by a grant from the Swedish Research Council, and this support is gratefully acknowledged.

REFERENCES

1. M. Abramowitz and I. A. Stegun, editors. *Handbook of Mathematical Functions.* Applied Mathematics Series No. 55. National Bureau of Standards, Washington D.C., 1970.
2. C. F. Bohren and D. R. Huffman. *Absorption and Scattering of Light by Small Particles.* John Wiley & Sons, New York, 1983.
3. R. de L. Kronig. On the theory of dispersion of X-rays. *J. Opt. Soc. Am.*, **12**(6), 547–557, 1926.
4. M. Gustafsson, C. Sohl, and G. Kristensson. Physical limitations on antennas of arbitrary shape. *Proc. R. Soc. A*, **463**, 2589–2607, 2007.
5. D. S. Jones. Low frequency electromagnetic radiation. *J. Inst. Maths. Applics.*, **23**(4), 421–447, 1979.
6. D. S. Jones. Scattering by inhomogeneous dielectric particles. *Quart. J. Mech. Appl. Math.*, **38**, 135–155, 1985.
7. R. E. Kleinman and T. B. A. Senior. Rayleigh scattering. In V. V. Varadan and V. K. Varadan, editors, *Low and high frequency asymptotics*, volume 2 of *Handbook on Acoustic, Electromagnetic and Elastic Wave Scattering*, chapter 1, pages 1–70. Elsevier Science Publishers, Amsterdam, 1986.
8. L. D. Landau and E. M. Lifshitz. *Statistical Physics, Part 1.* Butterworth-Heinemann, Linacre House, Jordan Hill, Oxford, third edition, 1980.
9. R. G. Newton. *Scattering Theory of Waves and Particles.* Dover Publications, New York, second edition, 2002.
10. W. K. Panofsky and M. Phillips. *Classical Electricity and Magnetism.* Addison-Wesley, Reading, MA, USA, second edition, 1962.
11. B. Peterson and S. Ström. T-matrix for electromagnetic scattering from an arbitrary number of scatterers and representations of E(3). *Phys. Rev. D*, **8**, 3661–3678, 1973.
12. C. Sohl and M. Gustafsson. A priori estimates on the partial realized gain of Ultra-Wideband (UWB) antennas. *Quart. J. Mech. Appl. Math.*, 2008. doi:10.1093/qjmam/hbn008.
13. C. Sohl, M. Gustafsson, and G. Kristensson. Physical limitations on broadband scattering by heterogeneous obstacles. *J. Phys. A: Math. Theor.*, **40**, 11165–11182, 2007.
14. C. Sohl, M. Gustafsson, and G. Kristensson. Physical limitations on metamaterials: Restrictions on scattering and absorption over a frequency interval. *J. Phys. D: Applied Phys.*, **40**, 7146–7151, 2007.
15. C. Sohl, C. Larsson, M. Gustafsson, and G. Kristensson. A scattering and absorption identity for metamaterials: experimental results and comparison with theory. *J. Appl. Phys.*, **103**(5), 054906, 2008.
16. C. Sohl. *Dispersion Relations for Extinction of Acoustic and Electromagnetic Waves.* Licentiate thesis, Lund University, Department of Electrical and Information Technology, P.O. Box 118, S-221 00 Lund, Sweden, 2007. http://www.eit.lth.se.
17. J. Van Bladel. *Electromagnetic Fields.* IEEE Press, Piscataway, NJ, second edition, 2007.
18. H. van de Hulst. *Light Scattering by Small Particles.* John Wiley & Sons, Inc., New York, 1957.
19. H. Wallén and A. Sihvola. Polarizability of conducting sphere-doublets using series of images. *J. Appl. Phys.*, **96**(4), 2330–2335, 2004.